Journal of Optics

PAPER

Ablated nickel nanoparticles: third harmonic generation and optical nonlinearities

To cite this article: Ke Zhang *et al* 2018 *J. Opt.* **20** 125502

IOP Publishing
Journal of Optics
J. Opt. **20** (2018) 125502 (11pp)
https://doi.org/10.1088/2040-8986/aaea4c

Ablated nickel nanoparticles: third harmonic generation and optical nonlinearities

Ke Zhang[1,2], **Sandeep Kumar Maurya**[1], **Rashid A Ganeev**[1], **Konda Srinivasa Rao**[1] and **Chunlei Guo**[1,3,4]

[1] The Guo China-US Photonics Laboratory, Changchun Institute of Optics, Fine Mechanics, and Physics, Chinese Academy of Sciences, Changchun 130033, People's Republic of China
[2] University of Chinese Academy of Sciences, Beijing 100049, People's Republic of China
[3] The Institute of Optics, University of Rochester, Rochester, NY 14627, United States of America

E-mail: rashid_ganeev@mail.ru and guo@optics.rochester.edu

Received 12 July 2018, revised 25 September 2018
Accepted for publication 22 October 2018
Published 8 November 2018

Abstract

We report the two-photon absorption and nonlinear refraction studies of the nickel nanoparticles (NPs) in deionized water using femtosecond laser pulses at 400 and 800 nm. The laser ablation technique was employed for the synthesis of nickel NPs using nanosecond, picosecond, and femtosecond pulses. The largest values of nonlinear absorption coefficients and nonlinear refractive indices were determined to be 9×10^{-11} cm W^{-1} and 2×10^{-15} cm^2 W^{-1} for smaller sized nickel NPs suspension. Third harmonic generation from the Ni plasma which contained NPs was analyzed using picosecond and femtosecond pulses as heating radiation and femtosecond probe pulses.

Keywords: nickel nanoparticles, third harmonic generation, nickel plasma, nonlinear refraction and absorption, optical limiting

(Some figures may appear in colour only in the online journal)

1. Introduction

Over the past few decades, metal nanoparticles (NPs) have been of great interest to the scientific community due to their exceptional optical properties, which have shown the potential application in a variety of the fields including biomedicine, electronics and energy technologies [1–7]. The vast amount of research work has been carried out for demonstration of the large nonlinear optical (NLO) response from NPs [8–13], which includes two-photon absorption (2PA) and nonlinear refraction (NLR). Various procedures such as vapor phase synthesis, thermal evaporation, electrochemical synthesis and chemical reduction synthesis have been used for preparation and studies of NPs [14, 15]. These preparation techniques do not apply efficiently to magnetic NPs such as iron, cobalt, nickel and titanium, whose metal ions are difficult to reduce for the formation of NPs due to their instability over the time.

The preparation of NPs has been mostly carried out using chemical reduction of their respective metal ions, which generally required the purification and stabilization of NPs after preparation. Meanwhile, the laser ablation (LA) can be efficiently applied for preparation of NPs that is much cleaner method and does not requires further purification [16, 17]. However, LA can also produce oxides, carbides and other species depending on the ambient medium, which can influence the properties of prepared NPs dispersed in respective solvents [18]. The formation of NPs primarily depends on the mechanisms involved in LA process. The sequence of these mechanisms include: (a) absorption of laser energy by metal surface which occurs on the femtosecond (fs) time scale, (b) energy transfer from excited electrons to acoustic phonons on the picosecond (ps) time scale, (c) thermal heating of the samples surface followed by mass vaporization on the nanosecond (ns) time scale, (d) generation of plasma on the surface followed by expansion and propagation of the generated shockwaves into the ambient environment, (e) plasma cooling and condensation of nano-sized particles and clusters, and (f) explosion and ejection of large particles on the

---

[4] Authors to whom any correspondence should be addressed.

microsecond time scale. Laser parameters, such as energy, wavelength and pulse duration, as well as sample properties including ambient environment, influence the above-mentioned mechanisms. In particular, the size and the shape of NPs can be controlled during LA by using pulses of different duration [19–23]. Therefore, the application of LA for preparation of NPs allows variation of their NLO properties by changing laser characteristics.

The studies of magnetic NPs were mostly concentrated on Fe, Ti and Co and their respective composite materials [10–12, 18]. This eventually led to the lack of information about optoelectronic properties of Ni NPs including their NLO parameters. Meanwhile, Ni NPs have attracted considerable interest due to their ferromagnetic properties [24–26], which can also modify their NLO characteristics. Most of the studies on Ni NPs have been carried out in their oxidized form or in composite materials [27, 28]. There are few reports on the LA of Ni in liquids using long laser pulses [29, 30]. The only study on the NLO response of Ni NPs, to the best of our knowledge, is presented in [31] where self-defocusing due to the thermo-optical properties and thermal heating effect have been shown. However, the electronic NLO response from Ni NPs induced by short pulses has not been reported so far, which promoted us to study these properties of Ni NPs under the influence of femtosecond laser excitation.

The LA in liquids is not the only technique used for preparation of NPs. Ni plasma formation in air can serve, particularly, as a nonlinear medium for harmonic generation in the plasma containing NPs. Earlier, the harmonic generation in plasma has been performed at vacuum conditions. The plasma created during LA contains electrons, atoms and molecules, ions, neutrals, clusters, quantum dots and NPs. The formation of NPs during plasma formation in ablation plume has been shown to significantly influence the efficiency of high-order harmonic generation [32]. At the same time, Ni NPs have been applied to study the low-order harmonic generation in microcube structures [33].

In this paper, we report the studies of NLO properties of Ni NPs prepared using LA in deionized water and air. The Z-scan technique was used to determine the 2PA coefficients and NLR indices under femtosecond excitation at 800 nm and 400 nm. We also report the third harmonic generation (THG) in Ni plasma in ambient air using picosecond and femtosecond heating pulses.

2. Experimental details

2.1. THG setup

We used the regenerative amplifier (Spitfire Ace, Spectra Physics) operating at 800 nm with the repetition rate of 1 kHz (figure 1(a)). We performed two sets of experiments where formation of plasma from Ni target was carried out using the 200 ps and 60 fs pulses ablating target in air, while pulse width of the probe laser beam was kept at 60 fs. Beam waist of these heating and probe pulses was fixed at 7 and 20 mm, respectively. Heating pulses reached the Ni target 38 ns before the probe pulses. The heating pulse was focused on the Ni target using 200 mm lens, whereas the probe pulse was focused using 300 mm lens parallel to the surface of the target and perpendicular to the propagation axis of heating pulse. The generated third harmonic (TH) radiation ($\lambda = 266$ nm) was separated from copropagating fundamental beam using dichroic filter and registered by a fiber spectrometer (Ocean Optics). The target was moved with constant speed to achieve the stable TH yield.

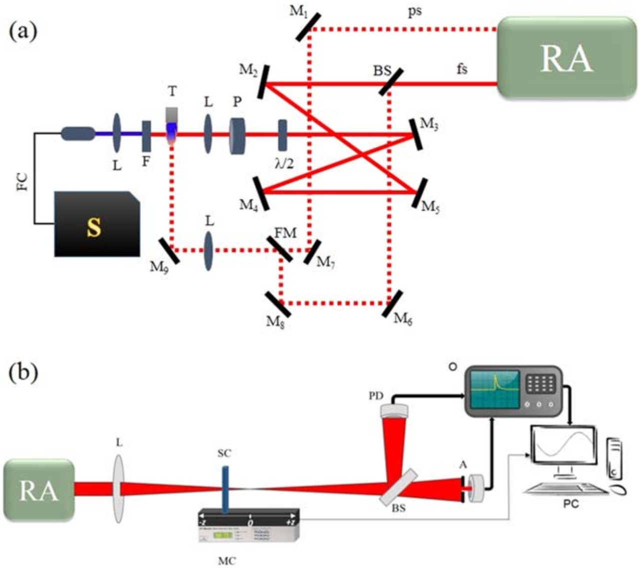

Figure 1. (a) Experimental setup for THG in the Ni plasma produced in air. Dotted lines represent heating beams and solid lines show the path of probe beam. (b) Z-scan scheme for the measurements of the optical nonlinearities of Ni NPs in water. RA: regenerative amplifier, M: reflecting mirrors, BS: beam splitter, FM: reflecting mirror on flip mount, L: lenses, P: polarizer, $\lambda/2$: half-wave plate, F: filter, T: target, S: spectrometer, FC: fiber cable, ps: picosecond radiation, fs: femtosecond radiation, MC: motion controller, SC: fused silica cell filled with nanoparticle suspension, A: aperture, PD: photo diode, PC: computer, O: oscilloscope.

2.2. Preparation of Ni NPs in deionized water

The ablation was carried out in deionized water using 60 fs and 200 ps pulses. The 6 ns pulses ($\lambda = 1064$ nm; Q-Smart, Coherent) were also used for ablation of the Ni target immersed in liquid. Laser pulse energies of 51, 0.542, and 0.596 mJ were used for ns, ps and fs ablation. Each ablation experiment was performed during 30 min. From here onward, we refer the prepared samples of Ni NPs suspensions as S_n, S_p, and S_f respectively for ns, ps, and fs ablation processes. The absorbance of Ni NPs suspensions was analyzed using spectrophotometer. The morphology of Ni NPs was studied using S-4800 (HITACHI) scanning electron microscope (SEM).

2.3. Z-scan scheme

The conventional Z-scan technique [34, 35] was employed to study the NLO properties of the Ni NPs in deionized water.

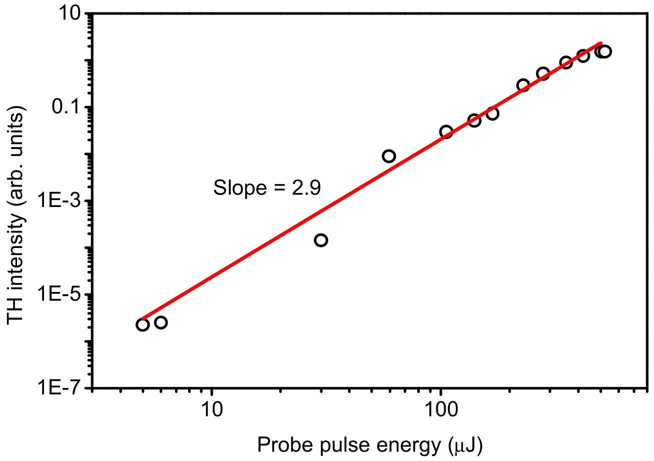

Figure 2. Variations of the intensity of the TH generated in air on the femtosecond probe pulse energy. The fitted solid line corresponds to the slope $l = 2.9$, which approximately corresponds to the cubic dependence of the harmonic yield on the probe pulse energy.

Schematic of the experimental setup is shown in figure 1(b). The pulse width of laser pulses at 800 and 400 nm was 60 fs. A 400 mm focal length lens was used to focus the laser beam into the quartz cell containing NPs. We employed open-aperture (OA) and close-aperture (CA) schemes for determination of 2PA coefficients (β) and NLR indices (γ), respectively. Sample cuvette of 2 mm path length was used during these studies. The cell was moved across the focal plane of the planoconvex lens along the beam propagation direction by means of motorized translational stage, which was interfaced with computer through EPS301 motion controller. The transmitted beam was measured by the large-area detectors (silicon photodiode, Thorlabs PDA100A-EC) through an aperture of 10% transmittance for CA scheme and 100% transmittance for OA scheme.

We fitted the following equations [34, 35] for normalized transmittance with experimental data

$$T_{2\mathrm{PA}}(z) = q^{-1} \times \ln(1 + q), \tag{1}$$

$$T_{\mathrm{NLR}}(z) = 1 + \frac{2(-\rho x^2 + 2x - 3\rho)}{(x^2 + 1)(x^2 + 9)}\Delta\phi_0. \tag{2}$$

Here, $q = \beta I_0 L_{\mathrm{eff}}/(1 + (z/z_0)^2)$, I_0 is the peak intensity of the laser pulse, z_0 is the Rayleigh length, $z_0 = k(w_0)^2)/2$, w_0 is the waist radius of focused beam, $L_{\mathrm{eff}} = [1 - \exp(-\alpha_0 L)]/\alpha_0$ is the effective length of the medium, α_0 is the linear absorption coefficient of medium, $\rho = \beta/2k\gamma$, $x = z/z_0$ and $k = 2\pi/\lambda$. $\Delta\phi_0$ is the phase change of the laser pulse due to NLR of the medium defined as $\Delta\phi_0 = k\gamma I_0 L_{\mathrm{eff}}$.

3. Results and discussion

3.1. THG in Ni NPs plasma

Prior to the study of harmonic generation in Ni plasma, the THG in air with variable probe pulse energy were performed, which showed the cubic dependence of harmonic yield on the laser energy as shown in figure 2. THG in air was carried out in order to calibrate our experimental setup.

A systematic study on the generation of the TH in the Ni plasma produced in air was performed using 800 nm probe pulses. We confirmed the presence of Ni NPs in plasma by analyzing the deposited materials from nearby substrates. We deposited the plasma debris on the glass and silicon substrates, which were further analyzed using the SEM. The SEM images clearly indicated the presence of the NPs, which were moved from the target towards the nearby substrate. From this observation, we concluded about the presence of Ni NPs in plasma. Meanwhile, the physical role of NPs in the harmonic generation is still debated [36]. One of unresolved problems is the concentration of the NPs produced during ablation at the moment of propagation of probe pulse through the spreading plasma. It is difficult to estimate the concentration of NPs in the plasma. There are several reports on the creation of NPs during ablation and estimations of their amount in laser-produced plasmas (for instance [37, 38]). It has been shown that concentration of smaller sized NPs in plasma is higher as compared to larger sized NPs. In our case, the particles with the sizes in the range of 5–60 nm were observed during the analysis of deposited debris.

In the first set of THG studies in plasmas, the 200 ps pulses were used as a heating radiation to create plasma. In the second case, both 60 fs heating and probe pulses were used. Under the experimental conditions with the heating energy of 163 μJ for ps pulses and 48.5 μJ for fs pulses, our first objective was to optimize the target position and the probe beam focal position to achieve the maximum TH from the Ni plasma. The TH intensities from the Ni plasma were determined by subtracting the measured TH intensities in air from TH intensities from the Ni plasma in air.

Figure 3(a) shows the variation of TH intensity as a function of the distance between the target and the propagation axis of the probe pulse. TH from Ni plasma was observed up to the distance of 3 mm away from Ni target with maximum harmonic intensity at 1.9 and 1.4 mm for the ps and fs heating pulses, respectively. TH intensity variations were symmetric around the maximal position of TH. The profile around TH maximal intensities can be explained by the fact that the change of the focal position leads to change in the spot size in plasma. At the constant pulse energy, the plasma plume showed a stream-like shape at smaller spot size, whereas the plasma plume exhibited the hemispherical structure at larger spot size. Earlier studies have shown the effect of spot size on the expansion of plasma. It has been demonstrated that the distribution of generated species during ablation is controlled by their longitudinal velocity, and strongly depends on input fluence [39, 40]. The distribution of different species during ablation has direct influence on the TH intensity with the change of the probe focal position that resulted in the maximal TH intensity away from target surface. This behavior of TH signal from Ni plasma using ps and fs heating pulses points out the importance of plasma expansion velocity during pulsed LA [41].

The inset in figure 3(a) depicts the TH intensity profile with varying spot size upon change of the focal plane of

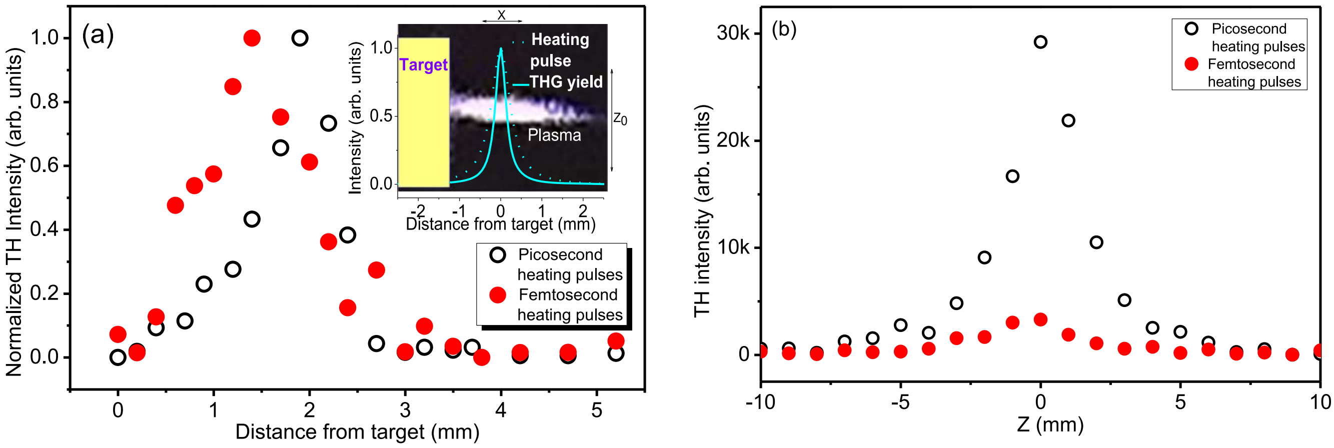

Figure 3. Variations of TH as the functions of (a) the distance between the target and the optical axis of the probe pulse at the constant heating pulse energies of 163 μJ (ps pulses, empty circles) and 48.5 μJ (fs pulses, filled circles) and (b) the position of the focal plane of probe pulse relative to the plasma at the constant heating pulse energies of 163 μJ (ps heating pulses, empty circles), 48.5 μJ (fs heating pulses, filled circles) and probe pulse energy of 30 μJ. Inset in figure 3(a) shows the scheme of TH variation versus distance of the probe pulse with respect to the target.

heating pulses. The spot size variation changes the fluence of heating pulses on the target surface during ablation, which eventually produces different concentration of plasma in the path of the probe beam. The image shows that there is a change in the intensity of the heating pulses at different positions of the target, which leads to the change of plasma concentration.

As it was mentioned, various species appear in the laser-produced plasma. These species with different velocities move towards the opposite direction with regards to the propagation of heating pulse. The size distribution of these species in the area of probe pulse propagation can be tuned by variation of the heating pulse energy and the delay between two pulses. The arrival of each species to the area of probe pulse propagation is different for different particles. Smaller sized particles arrive earlier than heavier particles. It has been shown that those species during ablation play different role in the THG [42]. Thus, the distribution of the NPs during ablation has direct influence on the THG efficiency. We did not carry out the delay dependent studies of harmonic yield. However, it can be assumed that, at the used delay between heating and probe pulses (38 ns), the most probable sources of harmonic generation were the single atoms and ions as well as a few-atomic species. Meanwhile, once one considers other mechanisms of energy transfer to NPs, like Coulomb explosion, their velocities may allow them to reach the area of driving pulse propagation during shorter time from the beginning of ablation. This consideration can be applied for the small NPs.

Figure 3(b) shows the dependence of the TH signal from the Ni plasma as a function of *z* position of the focused probe pulse at the pulse energy of 30 μJ. The energies of the ps and fs heating pulses were kept at 163 μJ and 48.5 μJ, respectively. These measurements were performed by analyzing different plasma regions at the fixed distance of probe beam (1.9 mm in the case of ps heating pulses and 1.4 mm in the case of fs heating pulses) relative to the Ni target. The relative efficiency of THG using ps heating pulses was notably higher compared to the fs heating pulses.

The variations of the TH intensity with variation of pulse energy of the heating and probe pulses were analyzed under the optimal conditions for TH from Ni plasma. The energies used for the formation of plasma were fixed at 163 μJ and 48.5 μJ for the ps and fs pulses, respectively. Figure 4(a) shows the TH yield from the Ni plasma increasing with the growth of the probe pulse energy. Variation of TH intensity shows approximately cubic dependence on the probe pulse energy up to ~50 μJ. At the constant probe pulse energy of 30 μJ, the TH intensity increases with the growth of heating pulse energy for both ps and fs heating pulses up to 600 μJ (figure 4(b)). TH monotonically increases with the increase of ps heating pulses energy, whereas for fs heating pulses, TH reaches saturation at the pulse energy of 200 μJ. The saturation can be caused by high concentration of free electrons in the Ni plasma produced by intense femtosecond heating pulses that lead to phase mismatch between the probe and TH waves [43].

Figure 5 shows the dependence of TH from the Ni plasma on the polarization of the probe beam. Under used experimental condition, the measured TH intensity has the uncertainty of about 10% with the variation of quarter wave plate. There could also be the 5% error in the definition of the angle of rotation of the quarter wave plate. The TH was maximal at linear polarization (at 0°) of the probe beam, whereas it completely disappeared in the case of circularly polarized light (i.e. at 45° rotation of the quarter-wave plate). The variation of the TH with the variation of polarization of the probe pulse is the characteristic of harmonic emission from isotropic materials, which depends as $I_{\mathrm{TH}} \propto \mathrm{Cos}\,(2\theta)$, where θ is the angle of rotation of the quarter-wave plate.

The plasma spectra from Ni ablation were analyzed to compare the fs and ps pulses induced plasma emission. As seen in figure 6, the relative intensity of plasma emission in the visible region is stronger for fs heating pulses compared to ps heating pulses. Contrary to that, in the UV region, the

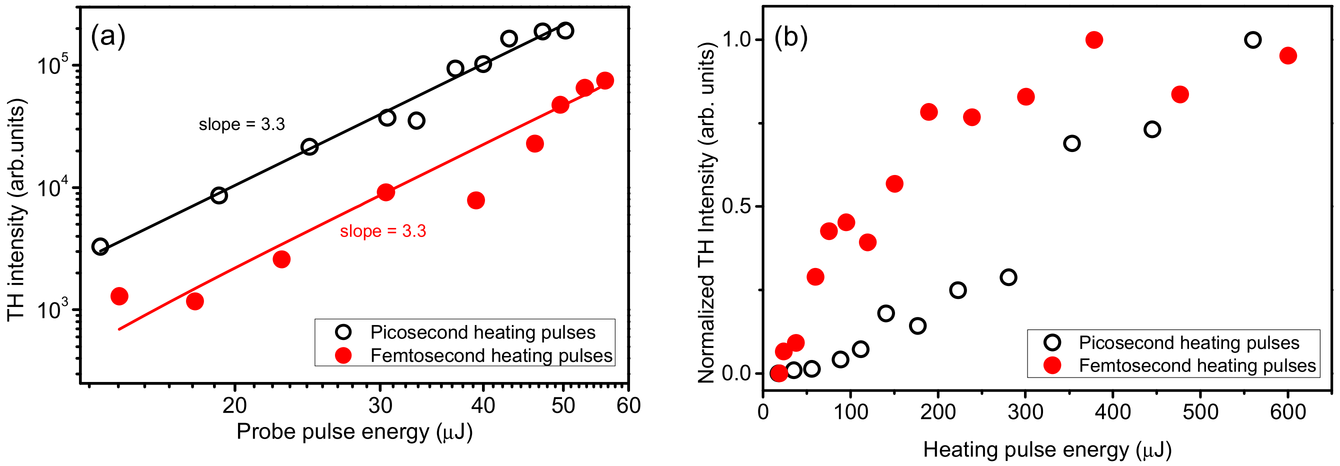

Figure 4. Variations of the TH in Ni plasma with (a) probe pulse energy at the constant heating energies of ps pulses (163 μJ, empty circles) and fs pulses (48.5 μJ, filled circle) and (b) heating energies of ps and fs pulses at the constant probe pulse energy of 30 μJ.

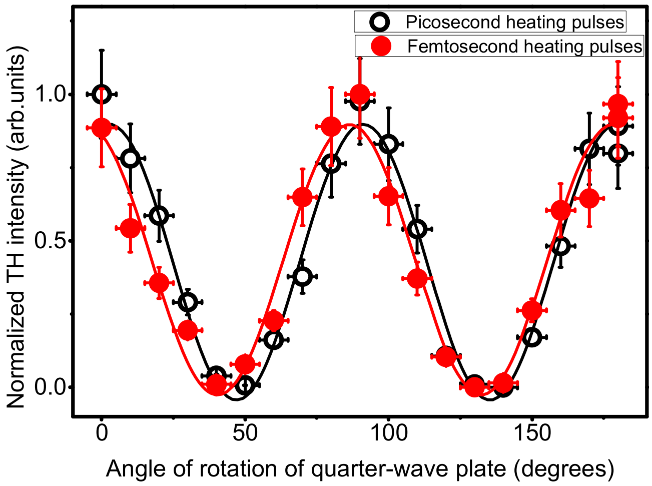

Figure 5. Variations of the TH generated in plasma with the angle of rotation of quarter-wave plate at the constant energies of ps heating pulses (163 μJ) and fs probe pulses (30 μJ). The pulse energy for fs heating pulses was 48.5 μJ. Solid curves represent the $I_{\mathrm{TH}} \infty$ Cos (2θ) dependences.

relative intensity is stronger for ps heating pulses compared to fs heating pulses. Spectral lines in the UV region (200–250 nm) mostly correspond to Ni II ions whereas most of the spectral lines in the visible region (300–550 nm) correspond to Ni I [44]. An additional line at 264.8 nm also appears in Ni plasma spectra with fs heating pulses. This emission was attributed to the TH, which disappears by changing the polarization of heating pulse from linear to circular.

3.2. Absorption spectra and SEM analysis of Ni NPs

Figure 7 shows the absorption spectra of ablated Ni NPs in deionized water. The absorption spectra show strong absorption close to 200 nm with the emergence of the broad absorption bands around 400 nm for all suspensions. Previously, various efforts have been made for explanation of appearance of the absorption band at 400 nm, which was assigned to the surface plasmon resonance (SPR) in Ni NPs [45, 46]. It has been explicitly shown the presence of two absorption bands in Ni NPs absorption spectra centered at 3.6 eV (345 nm) and 5.7 eV (217 nm) which were assigned to the SPR of Ni and interband d–d transition in Ni, respectively. Another reason for the existence of absorption band around 400 nm can be the oxidation of Ni NPs in deionized water that can lead to formation of NiO NPs [47–49]. They also exhibit the absorption band around 3.6 eV due to interatomic 3d–3d charge transfer. Hence the emergence of absorption band around 400 nm can be attributed to the coexistence of Ni and NiO NPs during LA in water. In the meantime, we notice the gradual enhancement of absorption starting from the longer wavelength region (i.e. between 400 and 700 nm).

The Ni NPs were characterized using SEM analysis. SEM images of Ni NPs show that the prepared NPs are spherical in shape as shown in figures 8(a)–(c). Their respective histograms are shown in figures 8(d)–(f). The mean size of NPs formed using fs laser pulse ablation was 50 nm (figures 8(c) and (f)) which is smaller compared to Ni NPs prepared using ps LA with the average particle size of 75 nm (figures 8(b) and (e)). This can be explained by the fact that two processes compete during ultrafast laser irradiation, which include columbic explosion and near-field enhancement at the surface of the NPs during ultrafast irradiation [20]. The columbic explosion is the dominant factor during femtosecond pulse irradiation compared to the picosecond laser irradiation where the effect of Coulomb explosion decreases [50] and the near-field enhancement occurs due to the energy imbalance in the NP surface [51]. Figure 9 shows the fluence dependence of NPs formation. The sizes of NPs were found to be the same irrespective of the variation of laser fluence of picosecond and femtosecond laser pulses.

The mean size of Ni NPs in S_n was smaller (23 nm, figures 8(a) and (d)) compared to the cases of ablation by ps and fs pulses (S_p and S_f). During irradiation by ns pulses, the photo-thermal effect [52, 53] becomes dominant compared to other processes of ablation causing the melting and evaporation at the surface of particle, which results in the temperature imbalance between the particle surface and bulk leading to the particle fragmentation. These processes can be

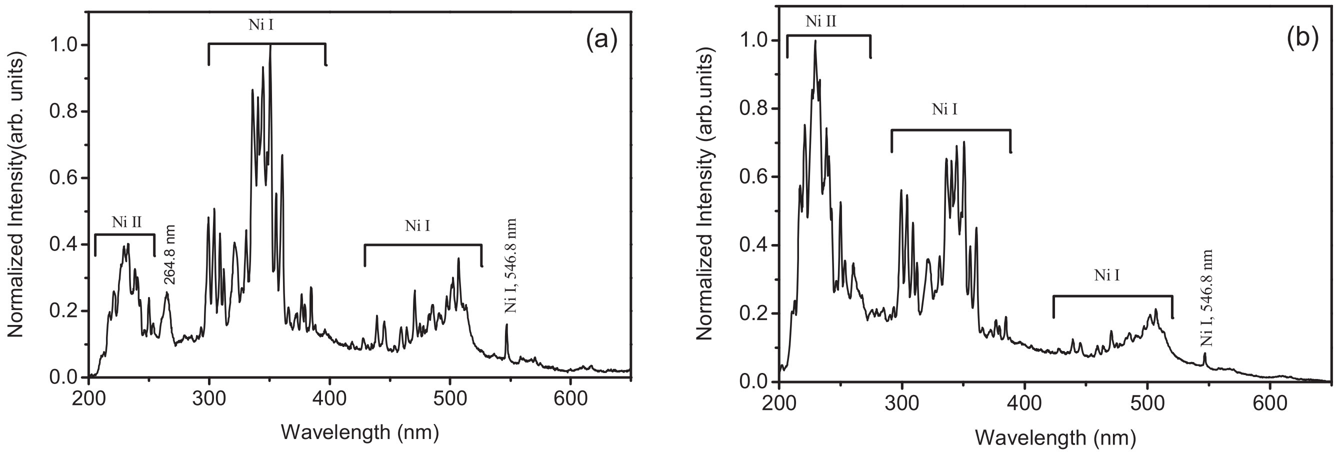

Figure 6. Spectra of plasma produced by (a) fs heating pulses (560 μJ) and (b) ps heating pulses (600 μJ) during ablation of Ni target.

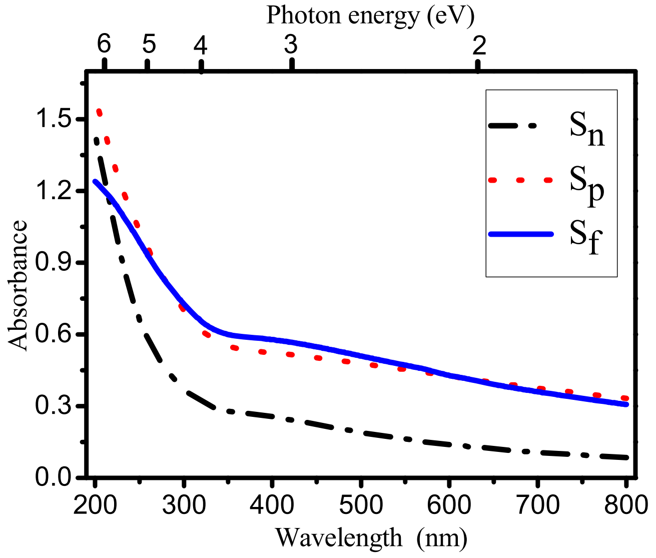

Figure 7. UV–vis spectra of Ni NPs in deionized water. Dashed dotted line represents the ns pulse ablation at 1064 nm, 10 Hz, dotted and solid lines represent suspensions prepared by ps and fs laser ablation at 800 nm, 1 kHz, respectively.

further influenced by thermal conductivity and thermal expansion coefficient of the Ni during photo-thermal fragmentation at ns pulses ablation [54]. During ns ablation, the temperature growth on the surface of Ni is much faster compared to the case of thermal expansion of the molten Ni, which can lead to smaller sized particles formation.

3.3. NLO properties of Ni NPs suspensions

The prepared Ni NPs suspensions were used to study their NLO properties by Z-scan technique at 800 and 400 nm. The OA Z-scan technique was employed to measure the 2PA coefficients. The results of studies are shown in figures 10(a)–(c) for 800 nm, 60 fs pulses (empty circles) and summarized in table 1. We also performed the Z-scan of deionized water at maximum applied fluence and did not observe the NLO response from this medium. It was found that S_p possesses slightly larger 2PA ($\beta = 2.1 \times 10^{-11}$ cm W^{-1}) compared to that for S_n and S_f (both 1.5×10^{-11} cm W^{-1}). NLO response of Ni NPs suspensions can be attributed to the influence of particle size [55], which is larger for S_p as compared to the S_n and S_f (see SEM images in figure 8).

It is worth mentioning that 800 nm wavelength falls in the tail of absorption spectrum for all ablated NPs (figure 7), which leads to low 2PA probability. Indeed, the steep growth of absorption appears in the UV region ($\leqslant$330 nm) of the spectrum of Ni NPs suspensions. However, the absorption starts to gradually grow from 500 nm towards shorter wavelengths in the visible region. Low nonlinear absorption using 800 nm probe pulses was caused by low 2PA due to relatively small linear absorption at 400 nm for three suspensions. However, it was not negligible to entirely exclude the 2PA process. To analyze the probability of the influence of higher-order NLO process, like three-photon absorption (3PA), on the Z-scans of our samples, we performed the intensity-dependent studies of the NLO properties of these NPs suspensions. During these studies, the β in all suspensions remained almost unchanged in the case of a two-fold growth of the probe pulse energy. Notice that 3PA characterizes by the relation $\beta \approx \beta_{2pa} + \beta_{3pa}I$, which shows the dependence of β on the probe pulse intensity (I). From our intensity-dependent studies, we concluded that the role of 3PA was insignificant compared with 2PA.

We also measured the NLR indices of S_n, S_p and S_f suspensions using femtosecond laser pulses (filled circles, figures 10(a)–(c)). These studies are summarized in table 1. The NLR at 800 nm shows the self-focusing properties at 1 kHz pulse repetition rate. This effect is related with Kerr-induced process rather than thermal processes since laser pulses are separated with the time of 1 ms, which is sufficient for dissipation of the absorbed energy from femtosecond laser pulses. The NLR indices were determined to be 6.6×10^{-16}, 5.4×10^{-16} and 6.6×10^{-16} cm^2 W^{-1} for S_n, S_p and S_f, respectively. The calculated NLR indices showed the reverse trend compared to 2PA coefficients. The value of γ was lower for S_p compared to the other two samples. The NLR of all studied samples was related to the contribution of intense laser pulse induced electronic polarization [56].

Z-scans were also performed at $\lambda = 400$ nm to analyze the influence of SPR in Ni NPs on the NLO characteristics of

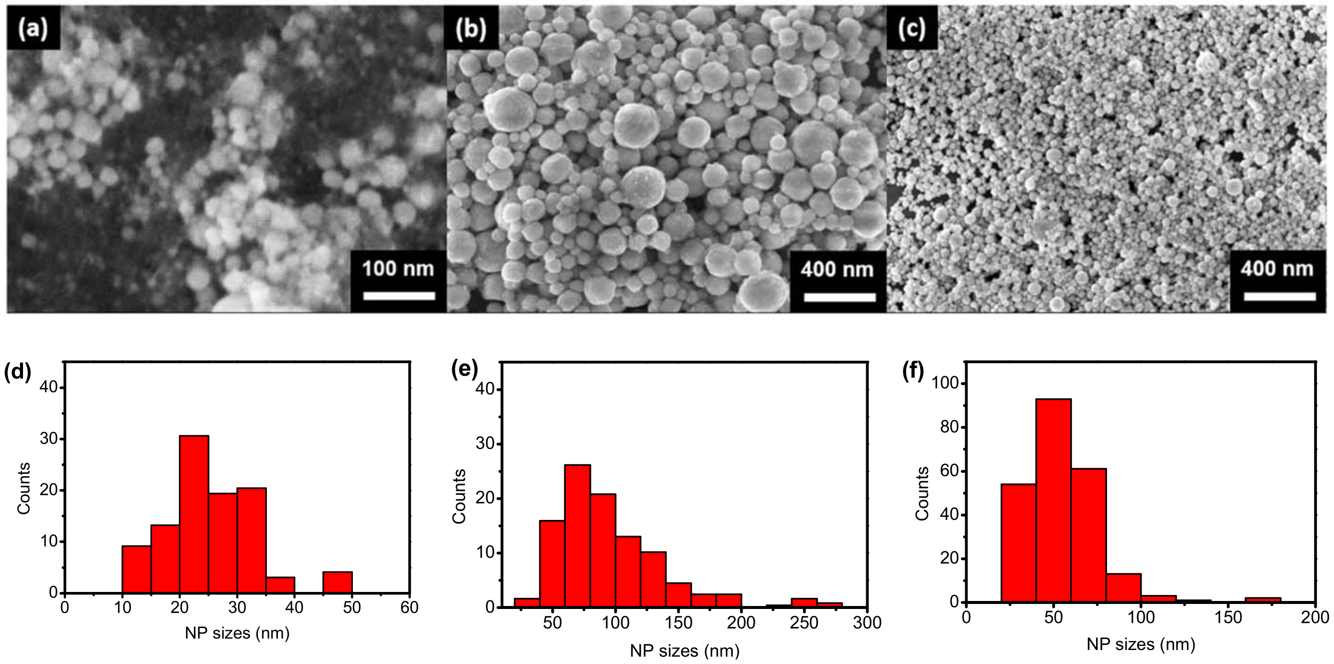

Figure 8. SEM images of the ablated Ni NPs in deionized water prepared using (a) 1064 nm, 5 ns, 10 Hz, (b) 800 nm, 200 ps, 1 kHz and (c) 800 nm, 60 fs, 1 kHz pulses. The respective size distributions of NPs are shown in (d)–(f).

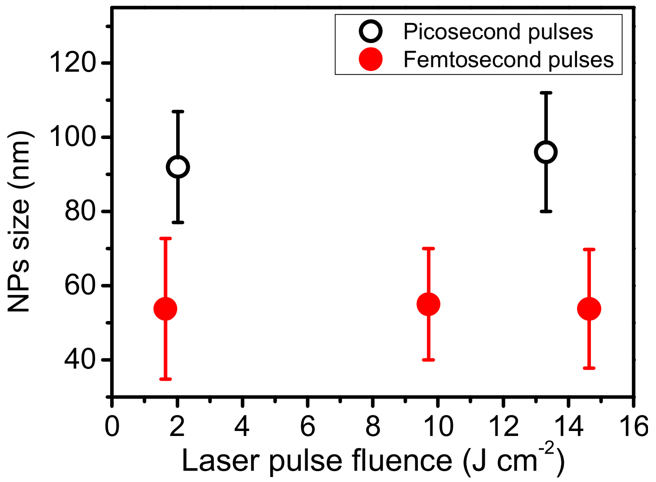

Figure 9. Average particle sizes of the synthesized Ni NPs as a function of laser fluence in the case of picosecond (empty circles) and femtosecond (filed circles) heating pulses.

these suspensions (figures 10(d)–(f)). At 400 nm, all NPs suspensions possessed higher 2PA and self-focusing compared to the same processes measured using 800 nm pulses (see table 1). The values of β were 9×10^{-11}, 4×10^{-11} and 6×10^{-11} cm W^{-1} for S_n, S_p and S_f, respectively. The study of NLR indices revealed the values of 2.1×10^{-15}, 1.6×10^{-15} and 1.4×10^{-15} cm^2 W^{-1} for S_n, S_p, and S_f, respectively.

Most of previous NLO studies of Ni NPs were carried out using CW or ns probe pulses in the visible region where they have shown the two orders of magnitude larger value of NLO as compared to the present study, due to the thermal lensing effect caused by extended probe pulse duration, contrary to our case when we used femtosecond radiation for the measurements of the NLO properties of Ni NPs suspensions.

The probable reason for higher NLO response from Ni NPs using shorter wavelength probe pulses is the influence of the broad absorption band at 400 nm and growing absorption of Ni at 200 nm. This can lead to the resonant two-photon excitation at 400 nm compared to the 800 nm, which has less probability for the 2PA. The excitation of NPs at 400 nm under the resonant conditions can give rise to the enhancement of NLO susceptibilities due to contribution from other resonances [57]. The creation of hot electrons can also influence the change in NLR at resonant conditions [58, 59]. Hence, the NLR index at $\lambda = 800$ nm is smaller due to the excitation wavelength, which is far from the SPR of Ni NPs.

Finally, we studied the optical limiting properties of different Ni NPs suspensions by varying the input fluence of 800 nm femtosecond pulses. For optical limiting measurements, the samples were placed at the focus of the lens in Z-scan setup. The input fluence was varied using the combination of half-wave plate and polarizer inserted in the path of laser beam.

The results of optical limiting studies in different Ni NPs suspensions are shown in figure 11. The presence of the plateau region was observed at a low incident fluence of laser pulses. The transmittance of Ni NPs suspension remained unchanged up to the input fluence of 8.7 mJ cm^{-2} for S_n, S_p, and S_f. Then the transmittance decreased upon the increase of input fluence above 8.7 mJ cm^{-2}. This observation led to the conclusion that, at the higher input fluence or intensity, the NPs suspension exhibits 2PA, as has been shown in our z-scan measurements.

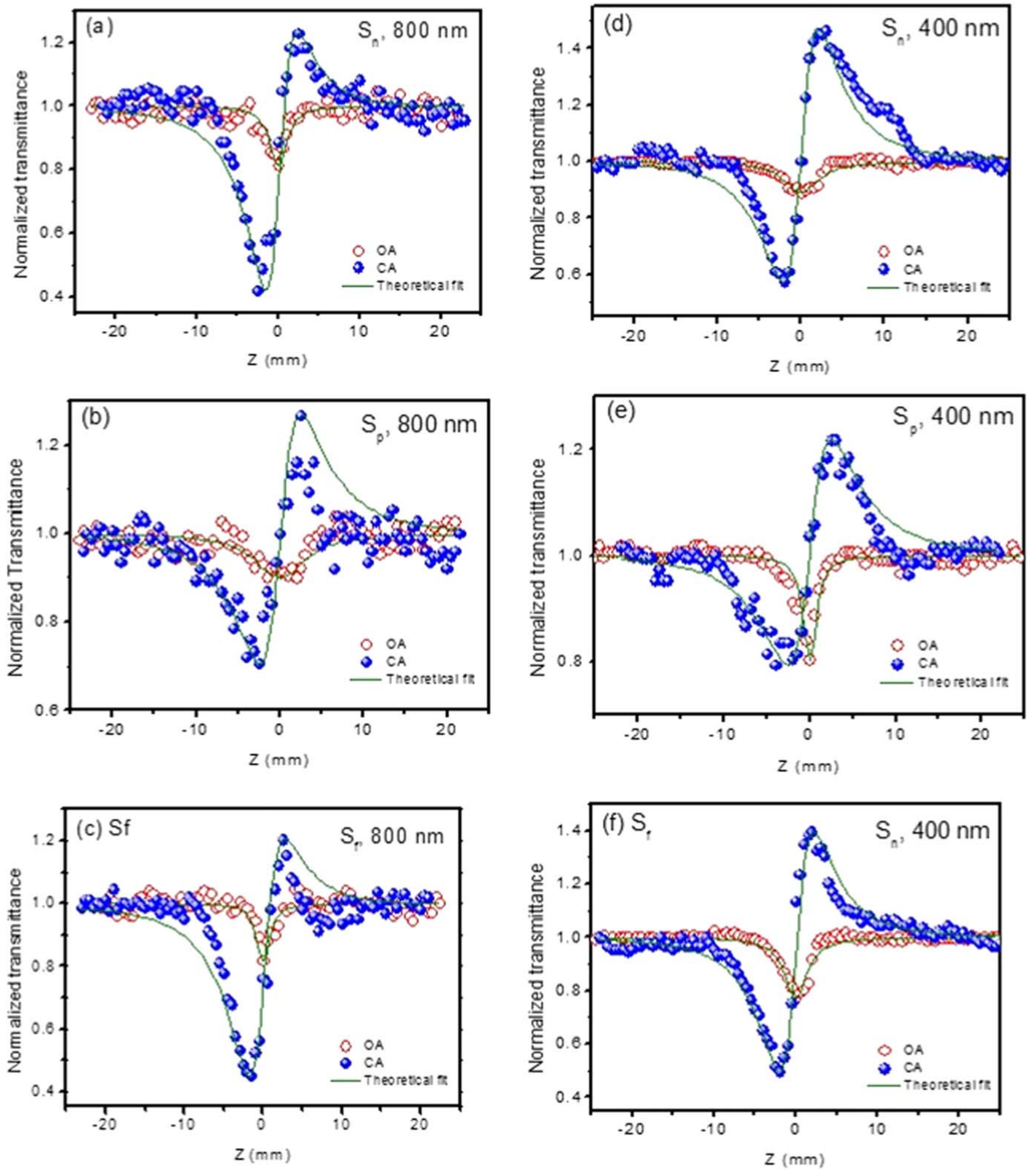

Figure 10. Z-scans of different Ni NPs in deionized water. (a)–(c) The Z-scan traces of S_n, S_p, and S_f using 800 nm radiation. Z-scan traces of S_n, S_p, and S_f using 400 nm radiation are shown in (d)–(f), respectively. Solid lines show the theoretical fits.

4. Conclusions

In conclusion, we have analyzed the NLO response of nickel NPs prepared using nanosecond, picosecond, and femtosecond pulse induced ablation in deionized water, as well as studied the lower-order harmonic generation in the plasma containing these NPs. Z-scan studies were employed for determination of the NLO properties using femtosecond pulses at 400 and 800 nm. The influence of NP size distribution on the NLO properties was observed at $\lambda = 800$ nm with the maximum 2PA coefficient of 2×10^{-11} cm W^{-1} for nickel NPs suspensions prepared using picosecond laser

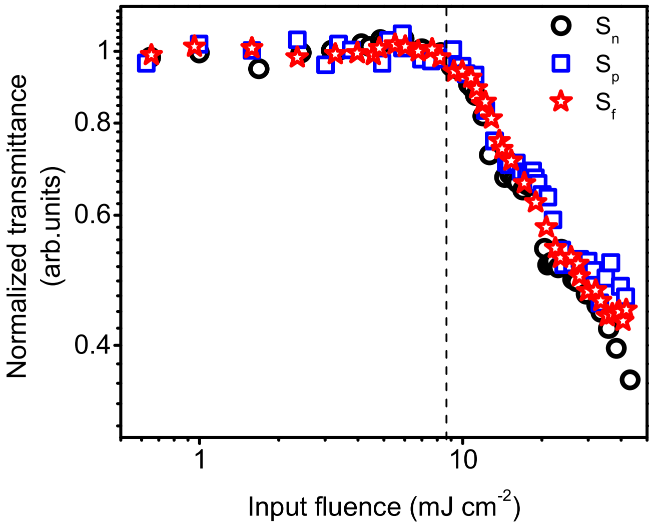

Figure 11. Optical limiting in S_n (empty circles), S_p (empty squares) and S_f (empty stars) using the 800 nm, 60 fs laser pulses.

Table 1. Nonlinear optical parameters of Ni NP suspensions prepared using laser ablation.

Wavelength, pulse duration	Sample	2PA coefficient (cm W^{-1})	Nonlinear refractive index (cm^2 W^{-1})
800 nm, 60 fs	S_n	1.5×10^{-11}	6.6×10^{-16}
	S_p	2.1×10^{-11}	5.4×10^{-16}
	S_f	1.5×10^{-11}	6.6×10^{-16}
400 nm, 60 fs	S_n	8.9×10^{-11}	2.1×10^{-15}
	S_p	4.2×10^{-11}	1.6×10^{-15}
	S_f	6.2×10^{-11}	1.4×10^{-15}

pulses. The larger 2PA coefficient of (9×10^{-11} cm W^{-1}) was measured for nickel NPs suspension at 400 nm, which was attributed to the influence of SPR. Similar to 2PA coefficients, NLR have shown larger indices at 400 nm as compared to the 800 nm. We also studied THG in nickel NP-containing plasma using 60 fs pulses at 800 nm. This study has shown that longer pulse duration of ablating radiation results in larger THG efficiency. Therefore, LA technique can provide efficient control over third-order optical nonlinearities, which can be modified by controlling the NP size formation during LA.

Acknowledgments

The financial support from National Natural Science Foundation of China (91750205), National Key Research and Development Program of China (2017YFB1104700) and Jilin Provincial Science & Technology Development Project (20180414019GH) is appreciated. R A G thanks the financial support from Chinese Academy of Sciences President's International Fellowship Initiative (Grant No. 2018VSA0001).

ORCID iDs

Sandeep Kumar Maurya https://orcid.org/0000-0003-4666-2168
Rashid A Ganeev https://orcid.org/0000-0001-5522-1802

References

[1] Tartaj P, Morales M P, Veintemillas-Verdaguer S, Gonzalez-Carreno T and Serna C J 2003 The preparation of magnetic nanoparticles for applications in biomedicine *J. Phys. D: Appl. Phys.* **36** R182–97

[2] Ganeev R A, Ryasnyansky A I, Stepanov A L and Usmanov T 2004 Saturated absorption and reverse saturated absorption of Cu:SuO$_2$ at $\lambda = 532$ nm *Phys. Status Solidi* b **241** R1–4

[3] Colombo M, Carregal-Romero S, Casula M F, Gutierrez L, Morales M P, Bohm I B, Heverhagen J T, Prosperia D and Parak W J 2012 Biological applications of magnetic nanoparticles *Chem. Soc. Rev.* **41** 4306–34

[4] Colodrero S, Ocaña M and Míguez H 2008 Nanoparticle-based one-dimensional photonic crystals *Langmuir* **24** 4430–4

[5] Gajc M, Surma H B, Klos A, Sadecka K, Orlinski K, Nikolaenko A E, Zdunek K and Pawlak D A 2013 Nanoparticle direct doping: novel method for manufacturing three-dimensional bulk plasmonic nanocomposites *Adv. Funct. Mater.* **23** 3443–51

[6] Flory F, Escoubas L and Bergine G 2011 Optical properties of nanostructured materials: a review *J. Nanotechnol.* **5** 052502

[7] Gao D, Ding W, Nieto-Vesperinas M, Ding X, Rahman M, Zhang T, Lim C and Qiu C-W 2017 Optical manipulation from the microscale to the nanoscale: fundamentals, advances and prospects *Light: Sci. Appl.* **6** e17039

[8] Huang J P and Yu K W 2005 Magneto controlled nonlinear optical materials *Appl. Phys. Lett.* **86** 041905

[9] Booth M J 2014 Adaptive optical microscopy: the ongoing quest for a perfect image *Light: Sci. Appl.* **3** e165

[10] Konopsky V N, Alieva E V, Alyatkin S Y, Melnikov A A, Chekalin S V and Agranovich V M 2016 Phase-matched third-harmonic generation via doubly resonant optical surface modes in 1D photonic crystals *Light: Sci. Appl.* **5** e16168

[11] Ganeev R A, Ryasnyansky A I, Stepanov A L and Usmanov T 2004 Characterization of nonlinear optical parameters of copper- and silver-doped silica glasses at $\lambda = 1064$ nm *Phys. Status Solidi* b **241** 935–44

[12] Baraskar P, Chouhan R, Agrawal A, Choudhary R J, Sen P K and Sen P 2018 Magnetic field induced changes in linear and nonlinear optical, properties of Ti incorporated Cr$_2$O$_3$ nanostructured thin film *Phys. Lett.* A **382** 860–4

[13] Ganeev R A, Suzuki M, Baba M, Ichihara M and Kuroda H 2008 Low- and high-order nonlinear optical properties of BaTiO$_3$ and SrTiO$_3$ nanoparticles *J. Opt. Soc. Am.* B **25** 325–33

[14] Mou X, Ali Z, Li S and He N 2015 Applications of magnetic nanoparticles in targeted drug delivery system *J. Nanosci. Nanotechnol.* **15** 54–62

[15] Cushing B L, Kolesnichenko V L and O'Connor C J 2004 Recent advances in the liquid-phase syntheses of inorganic nanoparticles *Chem. Rev.* **104** 3893–946

[16] Mafune F, Kohno J, Takeda Y and Kondow T 2001 Formation of gold nanoparticles by laser ablation in aqueous solution of surfactant *J. Phys. Chem.* B **105** 5114

[17] Ganeev R A, Baba M, Ryasnyansky A I, Suzuki M and Kuroda H 2005 Laser ablation of GaAs in liquids: structural, optical, and nonlinear optical characteristics of colloidal solutions *Appl. Phys.* B **80** 595–601

[18] Golightly J S, Castleman A W and Pennsyl V 2006 Analysis of titanium nanoparticle created by laser irradiation under liquids *J. Phys. Chem.* B **110** 19979–84

[19] Piriyawonga V, Thongpool V, Asanithia P and Limsuwan P 2012 Effect of laser pulse energy on the formation of alumina nanoparticles synthesized by laser ablation in water *Proc. Eng.* **32** 1107–12

[20] Jeon J-W, Yoon S, Choi H W, Kim J, Farson D and Cho S-H 2018 The effect of laser pulse widths on laser—Ag nanoparticle interaction: femto- to nanosecond lasers *Appl. Sci.* **8** 112

[21] Maximov K, Aristov A, Sentis M and Kabashin A V 2015 Size-controllable synthesis of bare gold nanoparticles by femtosecond laser fragmentation in water *Nanotechnology* **26** 065601

[22] Inasawa S, Sugiyama M, Noda S and Yamaguchi Y 2006 Spectroscopic study of laser-induced phase transition of gold nanoparticles on nanosecond time scales and longer *J. Phys. Chem.* B **110** 3114–9

[23] Amendola V and Meneghetti M 2009 Laser ablation synthesis in solution and size manipulation of noble metal nanoparticles *Phys. Chem. Chem. Phys.* **11** 3805–21

[24] Hinotsu T, Jeyadevan B, Chinnasamy C N, Shinoda K and Tohji K 2004 Size and structure of magnetic nanoparticles by using a modified polyol process *J. Appl. Phys.* **95** 7477–9

[25] Chinnasamy C N, Jeyadevan B, Shinoda K, Tohji K, Narayanasamy A, Sato K and Hisano S 2005 Synthesis and magnetic properties of face-centered-cubic and hexagonal-close-packed Ni nanoparticles through polyol process *J. Appl. Phys.* **97** 10J309

[26] Singh K, Kate K H, Chilukuri V V S and Khanna P K 2011 Glycerol mediated low temperature synthesis of nickel nanoparticles by solution reduction method *J. Nanosci. Nanotechnol.* **11** 5131–6

[27] Anthony J K, Kim H C, Lee H W, Mahapatra S K, Lee H M, Kim C K, Kim K, Lim H and Rotermund F 2008 Particle size-dependent giant nonlinear absorption in nanostructured Ni-Ti alloys *Opt. Express* **16** 11193–202

[28] Lu H and Wang W 2017 Picosecond nonlinear optical properties of $SrTiO_3$ composite films doped with gold and nickel nanoparticles *Appl. Opt.* **56** 4690–4

[29] Arboleda D M, Santillan J M J, Mendoza Herrera L J, Fernandez van Raap M B, Zelis P M, Muraca D, Schinca D C and Scaffardi L B 2015 Synthesis of Ni nanoparticles by femtosecond laser ablation in liquids: structure and sizing *J. Phys. Chem.* C **119** 13184–93

[30] Amoruso S, Bruzzese R, Wang X, NNedialkov N and Atanasov P A 2007 Femtosecond laser ablation of nickel in vacuum *J. Phys. D: Appl. Phys.* **40** 331

[31] Alikhani S, Tajalli H and Koushki E 2013 Third order optical nonlinearity and diffraction pattern of Ni nanoparticles prepared by laser ablation *Opt. Commun.* **286** 318–21

[32] Singhal H *et al* 2010 High-order harmonic generation in a plasma plume of *in situ* laser-produced silver nanoparticles *Phys. Rev.* A **82** 043821

[33] Ogata Y, Vorobyev A and Guo C 2018 Optical third harmonic generation using nickel nanostructure-covered microcube structures *Materials* **11** 501

[34] Sheik-Bahae M, Said A A and Van Stryland E W 1989 High-sensitivity, single-beam N_2 measurements *Opt. Lett.* **14** 955–7

[35] Sheik-Bahae M, Said A A, Wei T H, Hagan D J and Van Stryland E W 1990 Sensitive measurement of optical nonlinearities using a single beam *J. Quantum Electron.* **26** 760–9

[36] Ruf H *et al* 2013 Inhomogeneous high harmonic generation in krypton clusters *Phys. Rev. Lett.* **110** 083902

[37] Singh R P, Gupta S L and Thareja R K 2015 Third harmonic generation in air ambient and laser ablated carbon plasma *Phys. Plasmas* **22** 123302

[38] Noel S, Hermann J and Itina T 2007 Investigation of nanoparticle generation during femtosecond laser ablation of metals *Appl. Surf. Sci.* **253** 6310–5

[39] Wang Y, Chen A, Li S, Ke D, Wang X, Zhang D, Jiang Y and Jin M 2017 Influence of distance between sample surface and focal point on spectral intensity of nanosecond laser-induced silicon plasma in air *AIP Adv.* **7** 095204

[40] Li X, Wei W, Wu J, Jia S and Qiu A 2013 The influence of spot size on the expansion dynamics of nanosecond-laser-produced copper plasmas in atmosphere *J. Appl. Phys.* **113** 243304

[41] Claeyssens F, Ashfold M N R, Sofoulakis E, Ristoscu C G, Anglos D and Fotkis C 2002 Plume emissions accompanying 248 nm laser ablation of graphite in vacuum: effects of pulse duration *J. Appl. Phys.* **91** 6162

[42] Oujja M, Izquierdo J G, Banares L, de Nalda R and Castillejo M 2018 Observation of middle-sized metal clusters in femtosecond laser ablation plasmas through nonlinear optics *Phys. Chem. Chem. Phys.* **20** 16956

[43] Bulgakova N M, Bulgakov A V, Zhukov V P, Marine W, Vorobyev A Y and Guo C 2008 Charging and plasma effects under ultrashort pulsed laser ablation *Proc. SPIE* **7005** 70050C

[44] Kramida A, Ralchenko Y, Reader J and NIST ASD Team 2018 *NIST Atomic Spectra Database (version 5.5.6)* (Gaithersburg, MD: National Institute of Standards and Technology)

[45] Isobe T, Park S Y, Weeks R A and Zuhr R A 1995 The optical and magnetic properties of Ni^+-implanted silica *J. Non-Cryst. Sol.* **189** 173–80

[46] Amekura H, Kitazawa H, Umeda N, Takeda Y and Kishimoto N 2004 Nickel nanoparticles in silica glass fabricated by 60 keV negative-ion implantation *Nucl. Instrum. Methods Phys. Res.* B **222** 114–22

[47] Volkov V V, Wang Z L and Zou B S 2001 Carrier recombination in clusters of NiO *Chem. Phys. Lett.* **337** 117–24

[48] Kang T D, Lee H S and Lee H 2007 Optical properties of black NiO and CoO single crystals studied with spectroscopic ellipsometry *J. Korean Phys. Soc.* **50** 632–7

[49] Domingo A, Rodrıguez-Fortea A, Swart M, de Graaf C and Broer R 2012 *Ab initio* absorption spectrum of NiO combining molecular dynamics with the embedded cluster approach in a discrete reaction field *Phys. Rev.* B **85** 155143

[50] Werner D, Furube A, Okamoto T and Hashimoto S 2011 Femtosecond laser-induced size reduction of aqueous gold nanoparticles: *in situ* and pump-probe spectroscopy investigations revealing Coulomb explosion *J. Phys. Chem.* C **115** 8503–12

[51] Plech A, Kotaidis V, Lorenc M and Boneberg J 2006 Femtosecond laser near-field ablation from gold nanoparticles *Nat. Phys.* **2** 44–7

[52] Kawasaki M and Nishimura N 2006 1064-nm laser fragmentation of thin Au and Ag flakes in acetone for highly productive pathway to stable metal nanoparticles *Appl. Surf. Sci.* **253** 2208–16

[53] Werner D, Hashimoto S and Uwada T 2010 Remarkable photothermal effect of interband excitation on nanosecond laser-induced reshaping and size reduction of pseudospherical gold nanoparticles in aqueous solution *Langmuir* **26** 9956–63

[54] Abadlia L, Gasser F, Khalouk K, Mayoufi M and Gasser J G 2014 New experimental methodology, setup and LabView program for accurate absolute thermoelectric power and electrical resistivity measurements between 25 and 1600 K:

application to pure copper, platinum, tungsten, and nickel at very high temperatures *Rev. Sci. Instrum.* **85** 095121

[55] Ray P C 2010 Size and shape dependent second order nonlinear optical properties of nanomaterials and its application in biological and chemical sensing *Chem. Rev.* **110** 5332–65

[56] Boyd R W 2008 *Nonlinear Optics* 3rd edn (San Diego, CA: Academic)

[57] Smirnova D and Kivshar Y S 2016 Multipolar nonlinear nanophotonics *Optica* **3** 1241–55

[58] Guillet Y, Rashidi-Huyeh M and Palpant B 2009 Influence of laser pulse characteristics on the hot electron contribution to the third-order nonlinear optical response of gold nanoparticles *Phys. Rev.* B **79** 045410

[59] Hamanaka Y, Nakamura A, Hayashi N and Omi S 2003 Dispersion curves of complex third-order optical susceptibilities around the surface plasmon resonance in Ag nanocrystal-glass composites *J. Opt. Soc. Am.* B **20** 1227–32